Solid State Communications 250 (2017) 18–22

Contents lists available at ScienceDirect

Solid State Communications

journal homepage: www.elsevier.com/locate/ssc

Communication

Two single-layer porous gallium nitride nanosheets: A first-principles study

Hui Zhang[a], Fan-Sun Meng[b], Yan-Bin Wu[a,*]

[a] College of Sciences, Shenyang University, Shenyang 110044, China
[b] School of Science, Liaoning University of Technology, Jinzhou 121001, China

ARTICLE INFO

Keywords:
A. Gallium nitride
D. Electronic structure
E. First-principles calculations

ABSTRACT

The gallium nitride (GaN) is a novel wide-gap semiconductor for photoelectric devices. In this paper, two 2D single-layer GaN crystal structures, called H–GaN and T–GaN, are discovered by the density functional theory calculations. The phase stability is confirmed by phonon dispersions. The sole-atom-thick crystals of H–GaN and T–GaN, has possess enlarged specific surface area than the graphene-like allotrope (g-GaN) due to the porous structures. In addition, they have indirect band gaps of 1.85–1.89 eV and the electronic structures can be further modulated by applied strains. For example, T–GaN transforms from an indirect semiconductor to a direct one due to compressed strains. Both the combination of high specific surface area and moderate band gaps make these 2D crystals potential high-efficiency photocatalysts. Our results will also stimulate the investigations on 2D GaN nano crystals with rich electronic structures for wide applications.

1. Introduction

Investigations on the two-dimensional (2D) nanocrystals with atomic-thickness, such as representative graphene, have been the most active field since the discovery of graphene. The single-layer graphene possesses many excellent quantum transport and mechanical properties [1,2], which is consequently considered one of the most promising materials for future electronics. Nevertheless, the absence of intrinsic band gap, which greatly hampers more wide application of graphene [3], has stimulated exploration of other 2D nanomaterials, such as C_3N_4, phosphorus allotropes and transition metal dichalcogenides (TMDs) [4–9].

Among diverse 2D materials, many 2D BN counterparts have been theoretically explored and experimentally studied [10,11]. Beyond graphene-like 2D materials, the 2D porous films and nanomaterials [12–15], including porous BN nonosheets [16,17], have been recently fabricated as high-performance catalysts, due to extremely high specific surface area and special surface activity [18,19]. However, the 2D forms of AlN and GaN, which belongs to well-known III–V semiconductors for the device applications as well as BN, have seldom been fabricated [20]. Bulk GaN is a wide-gap (~3.5 eV) semiconductor that usually crystallizes in the wurtzite lattice [21]. The graphene-like 2D g-AlN and g-GaN nanosheets have been demonstrated as free-standing [22,23] due to theoretical calculations. Recently, the synthesis of 2D gallium nitride (GaN) has been reported via a migration-enhanced encapsulated growth (MEEG) technique utilizing epitaxial grapheme [24]. In addition, porous GaN polycrystalline structures have been experimentally formed [25–27]. Based on the previous findings, it is interesting to explore 2D porous GaN crystals with novel electronic strctures.

In this paper, the feasibility of fabricating porous monocrystalline of GaN is explored by systematic first-principles calculations based on the density functional theory. Two periodic single-layer H–GaN and T–GaN nanosheets are demonstrated as free-standing stable. They possess especially high specific surface area. Furthermore, they are semiconductors and their band gaps can be modulated by mechanical strains. All these superior properties suggest future applications in photo electronic fields.

2. Methodology

The first-principles calculations were performed with the Vienna Ab Initio Simulation Package (VASP) [28,29]. The electron exchange correlation interactions were treated by as generalized gradient approximation (GGA) with the Perdew-Burke-Ernzerhof (PBE) functional [30], by using the Projector-augmented-wave (PAW) potentials [31], which account for the electron-ion interactions. To remove spurious interactions between neighboring structures due to periodic calculations, a vacuum layer of no less than 12 Å was taken in the perpendicular direction. The energy cutoff was set to 600 eV and the Monkhorst-Pack scheme for k-meshes was used to sample the Brillouin zone (BZ) [32].

The equilibrium geometries were fully optimized with both the lattice vectors and atom coordinates relaxed until forces on them

* Corresponding author.
E-mail address: yanbinwu@outlook.com (Y.-B. Wu).

http://dx.doi.org/10.1016/j.ssc.2016.11.011
Received 8 September 2016; Received in revised form 11 November 2016; Accepted 12 November 2016
Available online 13 November 2016

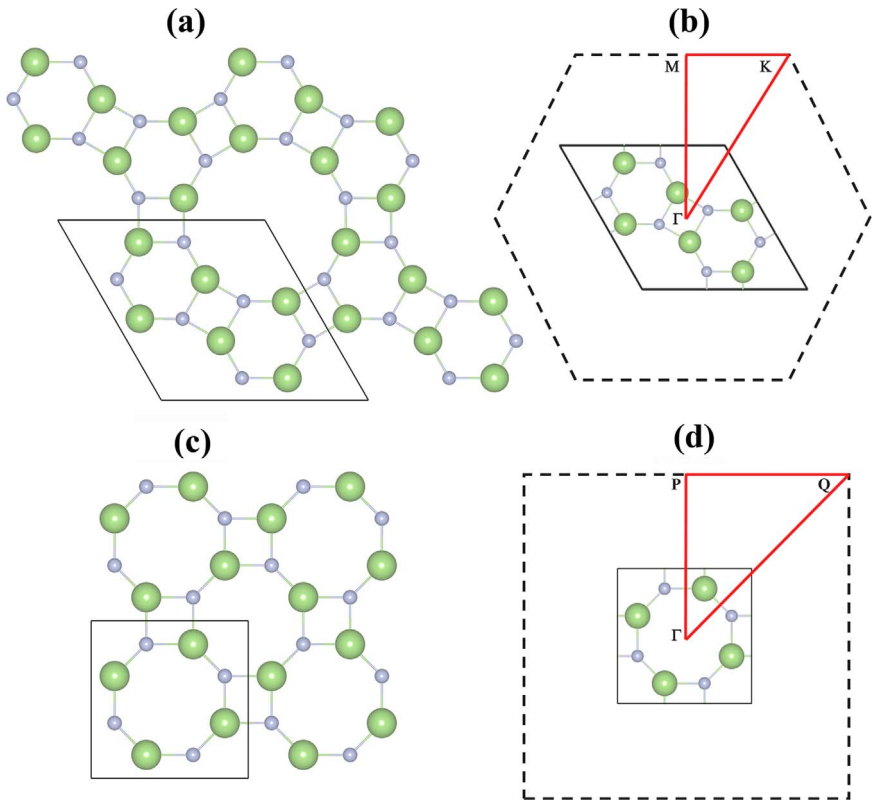

Fig. 1. Color online: The (a) atomic configuration and (b) first Brillouin zone of H–GaN, respectively. The results of T–GaN are shown in (c) and (d). The green and gray balls represent the Ga and N atoms, respectively.

became less than 0.01 eV/Å on each atom. The phonon calculations were performed by using the Phonopy package [33]. The real-space force constants were calculated from the Hellmann-Feynman forces by introducing displacements to supercells based on finite displacement method [34], and the dynamical matrices and phonon frequencies were obtained via the force constants.

3. Results and discussion

3.1. Atomic structures and stability

The structures originate from two previous carbon allotropes predicted in 2012, which are called porous graphene and T graphene, respectively [35,36]. In this work, two GaN polymorphs are considered by alternately replacing C atoms by Ga and N atoms. After fully optimization, one structure has a hexagonal lattice, which is named as H–GaN, and the other one has a tetragonal lattice, which is called as T–GaN, as shown in Fig. 1(a) and (c), respectively. The H–GaN and T–GaN belong to 175.P6/M(C6H-1) and 127.P4/MBM(D4H-5) point group symmetry, respectively. In the two structures, each N (Ga) atom is surrounded by three nearest-neighbor Ga (N) atoms, which is exactly as graphene and *h*-BN. It has to be noted that the present T–GaN has previously been reported [37] in 2015 which was called as the Haeckelite structure.

For H–GaN and T–GaN structures, 6×6×1 and 8×8×1 k-meshes are automatically generated. To confirm the calculation reliability, the calculations are compared with previous results. For example, the calculated lattice constant of bulk wurtzite GaN is a=3.25 Å and c=5.28 Å, which agrees well the previous results of a=3.22 Å and c=5.23 Å with PBE function [38]. The equilibrium lattice constants of monolayer H–GaN and T–GaN are 8.86 and 6.41 Å, respectively. The Ga–N bond length in present 2D structures is around 1.83 Å, which is a little smaller than that of 1.98 Å in bulk one.

The present 2D GaN nano crystals form big porous circles, as shown in Fig. 1, where H–GaN has circles with twelve atoms and T–GaN has ones with eight atoms. As a result, they could have higher specific surface area than graphene-like GaN. The ideal specific surface area of is H–GaN and T–GaN is 1620 m^2/g and 2200 m^2/g, respectively. The specific surface area is dramatically enlarged compared with that of (437 m^2/g) g-GaN. In fact, the specific surface area of T–GaN is only a little smaller than that (2630 m^2/g) of Graphene. Extraordinary high specific surface area of H–GaN and T–GaN crystals makes them underlying catalysts due to higher effective reaction area.

The phonon dispersion spectrum analysis is a reliable tool to confirm the structure stability. A crystal structure could be considered as stable when all its phonon frequencies on the k-points in the Brillouin zone are positive [39,40]. As a result, accurate phonon calculations were performed to further check the structure stabilities. In phonon calculations, 4×4 supercells are employed, which contains total 192 and 128 atoms for H–GaN and T–GaN, respectively. The Brillouin zone is sampled by 4×4 *k*-meshes. The phonon dispersions are depicted along the high-symmetry directions, as shown in Fig. 2(a) and (b) for H–GaN and T–GaN, respectively. The results show that all phonon frequencies are positive and thus these two monolayers can be considered as thermaldynamically stable.

Beside phonon analysis, the phase stability of 2D materials can also be determined from the formation energy. In principle, lower formation energy of a 2D crystal indicates it is easier to be exfoliated from bulk counterparts and has better phase stability in 2D forms. The formation energy of single-layer GaN is calculated as$E_f = E_{SL}(GaN) - E_{Bulk}(GaN)$, where $E_{SL}(GaN)$ and $E_{Bulk}(GaN)$ represent the total energies per atom of single-layer and bulk wurtzite GaN structures, respectively, The formation energies of H–GaN and T–GaN are 0.061 and 0.055 eV, respectively, which are a little higher than that (0.042 eV) of graphene-like g-GaN due to the porous structure. However, the formation energies of present monolayers are both lower than that (0.078 eV) of single-layer MoS_2 [41]. As single-layer MoS_2 nanosheets have been successfully fabricated [42], these porous GaN

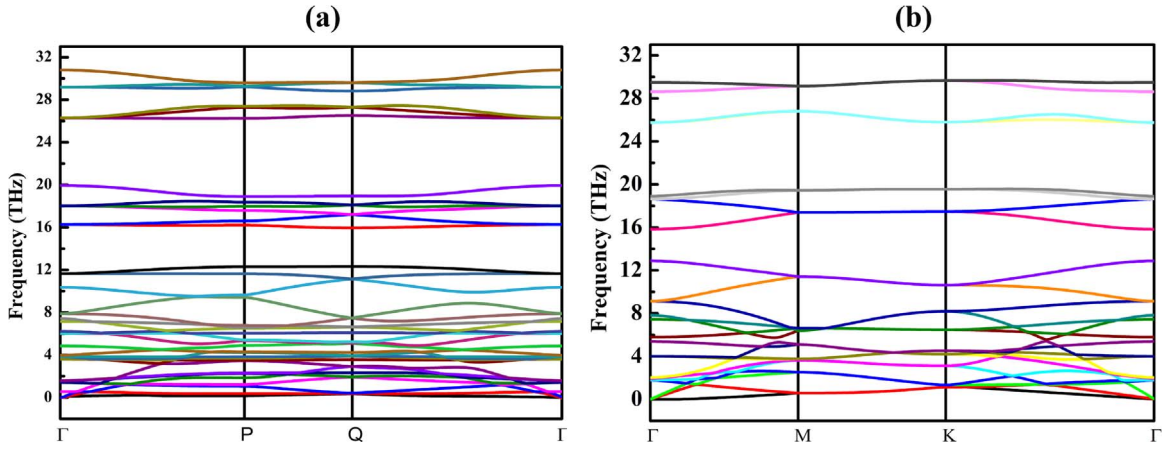

Fig. 2. Color online: The phonon dispersions of (a) H–GaN and (b) T–GaN, respectively.

crystals can also be expected to be synthesized experimentally in the future.

3.2. Electronic structures

After determining the phase stability, it is natural to explore whether these two GaN allotropes have any unique electronic structures for applications. The electronic band structures indicate that both of them are indirect semiconductors, as shown in Fig. 3. The band gaps are around 1.85–1.89 eV, and shows no big difference for the two crystal structures. In addition, the band gaps of present structures are a little smaller than that 2.00 eV of graphene-like g-GaN [23] and that 1.92 eV [38] of bulk wurtzite one with the same PBE functional.

As the typical DFT with GGA functional usually underestimates the band gap due to the spurious electronic self-interaction, herein we also supplemented the Heyd-Scuseria-Ernzerhof (HSE06) hybrid functional which could usually predict more reasonable band gaps than GGA. The calculations show that the band gap is enlarged to be 3.10 and 3.12 eV for H–GaN and T–GaN, respectively. The HSE function calculations do not change the trend but only give larger gaps. The issue is reasonable because overestimated gaps by HSE than those by GGA usually happen, e.g. 2.05 eV by HSE being compared with 1.60 eV by PBE [43] for single-layer MoS_2.

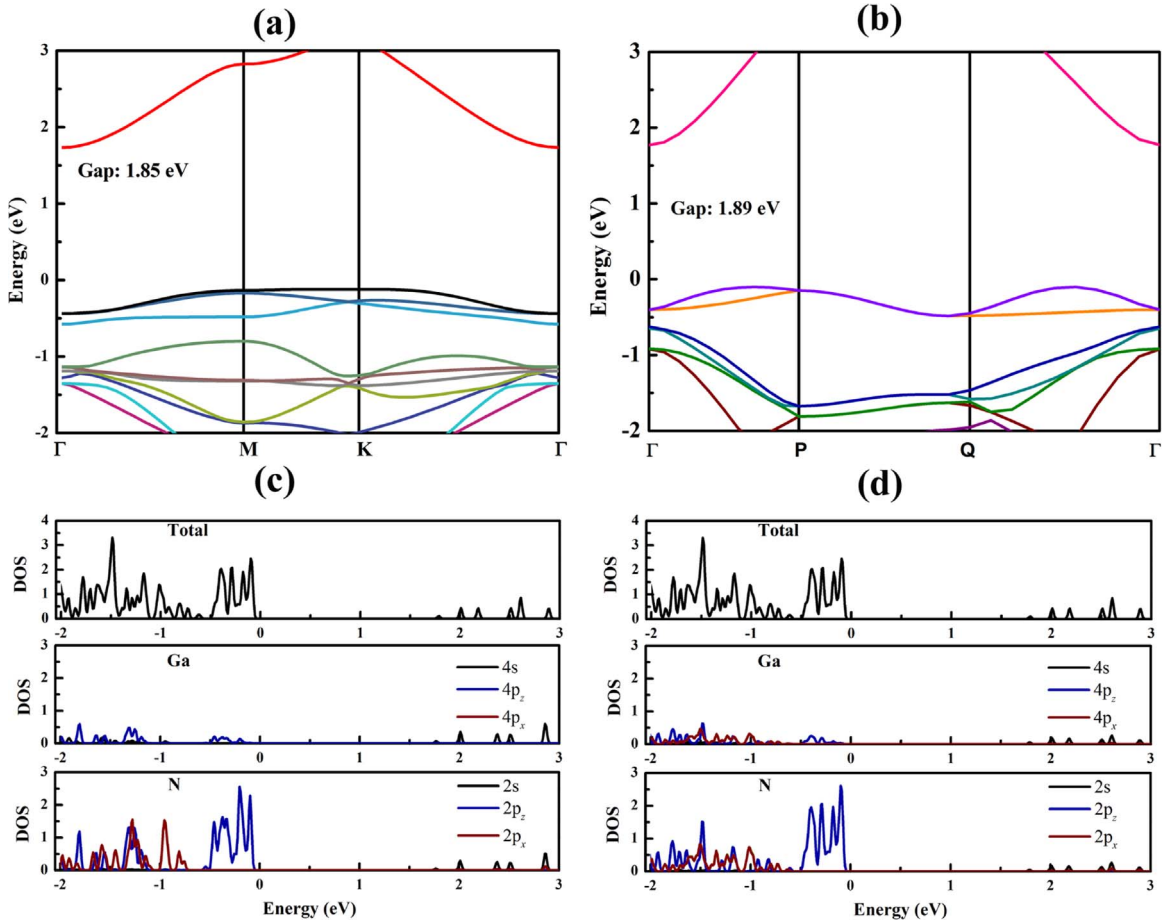

Fig. 3. Color online: The electronic band structures in (a) and (b), along with the projected density of states in (c) and (d), for H–GaN and T–GaN, respectively..

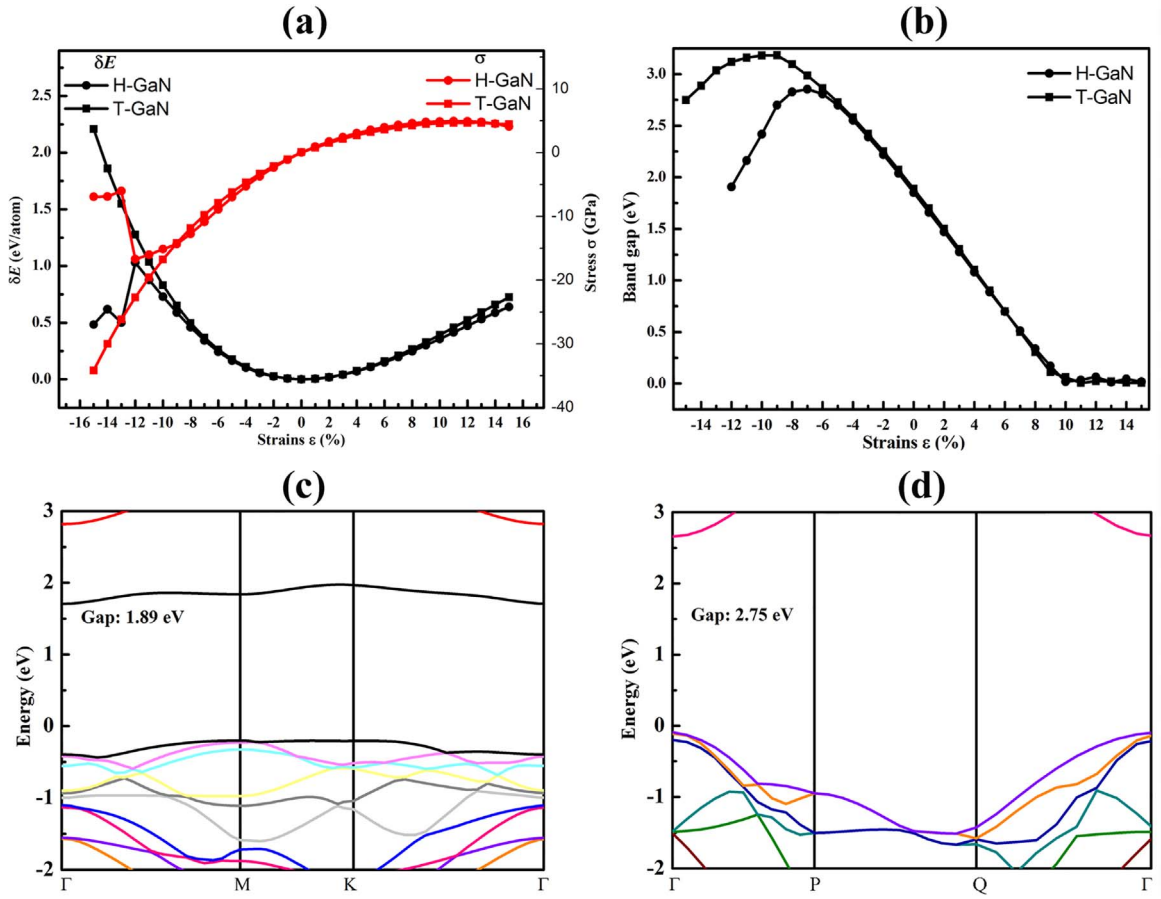

Fig. 4. Color online: Strain effects on porous GaN compounds. The energy difference and stresses are shown in (a), and the band gaps variation is shown in (b). The electronic band structures of compressed H–GaN (ε=−12%) and T–GaN (ε=−15%) in (c) and (d) respectively..

3.3. Strain effects on electronic structure

Tunable electronic structure is an important property for semiconductors, which can expand their application range. The electronic structures have been previously demonstrated to be modulated from many routes, such as defects and electric fields [44,45]. In addition, it is a well-known method to modulate the band gap via mechanical strains because it is precisely controllable. Herein, the strain effect on the electronic structure of 2D GaN monolayers are investigated.

For comparison, both the compression and tension strains (maximum ε= ± 15%) are applied with the step of 1%. The energy change due to strains is defined as:$\delta E = E_s - E_p$, where E_s and E_p represent total energy of the strained and prefect 2D GaN, respectively. Both the energy and stress are shown in Fig. 4(a) to analyze the stability under different strains. The energy changes with a parabolic curve for T–GaN for all strains, which indicate the elastic deformation. Hoverer, the maximum compressed strain for H–GaN is ε=−12% due to sudden energy drop, which indicates bigger strains are away from elastic deformation. The stress change provides the similar trend due to the discontinuity at ε=−12%. As a result, the electronic structures are considered for H–GaN at strains ε=−12–15%.

The band gaps of H–GaN are decreased for tensile strains but are increased by compressed ones, as shown in Fig. 4(b). In addition, H–GaN arrive at a maximum band gap of 2.8 eV for compressed strains around −7%, and transforms to be metallic for tensile strains bigger than 10%. The T–GaN shows a similar electronic structure changing behavior under changing strains. Specially, T–GaN becomes a direct semiconductor from indirect one at compressed strains bigger than ε=−8% and the band gap is 2.75 eV (Fig. 4(d)) at maximum ε=−15%. Thus, these two 2D structures are gap-tunable semiconductors due to strains, and also can become metallic at large strains.

3.4. Optical absorption index

In solar energy spectrum, the infrared radiation and visible light account for over 90% of energy. As a result, candidates for solar energy applications such as photocatalytic applications demand a wide adsorption range of solar energy. The optical absorption coefficients directly reflect the absorption range of the spectrum and are critical in solar energy conversion realm. Based on calculating the imaginary part of the complex dielectric function, the optical adsorption spectrum are obtained [46], which directly reflect the absorption range of the spectrum.

The two structures has very small absorption index, as shown Fig. 5. This indicates extremely low energy utilization efficiency like

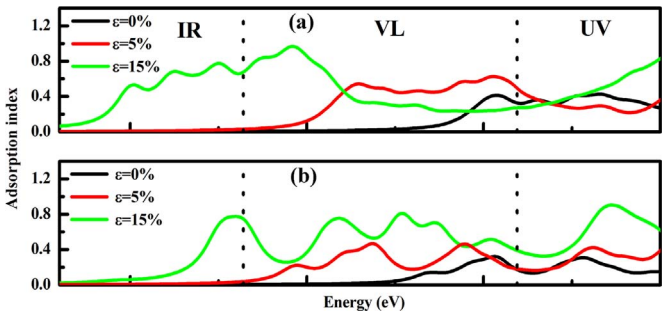

Fig. 5. Color online: The optic adsorption index of upper H–GaN and lower T–GaN under different tensile strains. The regions represented as IR, VL and UV are the energy range of infrared radiation, visible light and ultraviolet radiation, respectively.

wide-band gap TiO_2 [47,48]. Furthermore, the absorption spectrums of two crystals are red-shifted at tensile strains and shows considerable absorption index in IR and VL regions. The results show that the solar energy utilization efficiency of porous GaN crystals can be raised by the applied strains.

4. Conclusions

In this paper, systematic first-principle calculations were performed to explore the phase stability, electronic and optical properties of 2D GaN nano materials. The two H–GaN and T–GaN have been demonstrated as stable due to accurate phonon dispersion calculations. Both H–GaN and T–GaN crystals are indirect semiconductors with gap of 1.85–1.89 eV. Interestingly, the electronic structure shows strain-dependence and can become metallic under tensile strains. In addition, T–GaN changes from an indirect semiconductor to a direct one. Our theoretical results not only declare new porous crystal structures of GaN, but also provide a novel way to obtain high specific surface area for nano materials, which may greatly help to explore new catalysts in the future.

Acknowledgments

The authors acknowledge the financial support by National Natural Science Foundation of China (no. 11547115) and Science Research Foundation for PhD of Liaoning Province (201501091). The computations supports from Informalization Construction Project of Chinese Academy of Sciences during the 11th Five-Year Plan Period (no. INFO-115-B01) are also highly acknowledged.

References

[1] C.N.R. Rao, H.S.S. Ramakrishna Matte, U. Maitra, Angew. Chem. Int. Ed. 52 (2013) 13162–13185.
[2] M.S. Xu, T. Liang, M.M. Shi, H.Z. Chen, Chem. Rev. 113 (2013) 3766–3798.
[3] J.F. Gao, J.J. Zhao, F. Ding, J. Am. Chem. Soc. 134 (2012) 6204–6209.
[4] Q. Liu, J. Zhang, Langmuir 29 (2013) 3821–3828.
[5] A.S. Rodin, A. Carvalho, A.H. Castro Neto, Phys. Rev. Lett. 112 (2014) 176801.
[6] Z. Zhu, D. Tománek, Phys. Rev. Lett. 112 (2014) 176802.
[7] Q. Tang, Z. Zhou, Prog. Mater. Sci. 58 (2013) 1244–1315.
[8] Q. Tang, Z. Zhou, Z.F. Chen, WIREs Comput. Mol. Sci. 5 (2015) 360–379.
[9] Q. Tang, Y. Cui, Y.F. Li, Z. Zhou, Z.F. Chen, J. Phys. Chem. C. 115 (2011) 1724–1731.
[10] X.X. Li, J. Zhao, J.L. Yang, Sci. Rep. 3 (2013) 1858.
[11] X.G. Luo, L.-M. Liu, Z.P. Hu, W.-H. Wang, W.-X. Song, F.F. Li, S.-J. Zhao, H. Liu, H.-T. Wang, Y.J. Tian, J. Phys. Chem. Lett. 3 (2012) 3373–3378.
[12] J. Su, X. Zou, G.-D. Li, Y.-M. Jiang, Y. Cao, J. Zhao, J.-S. Chen, Chem. Commun. 49 (2013) 8217–8219.
[13] Z. Lu, H. Zhang, W. Zhu, X. Yu, Y. Kuang, Z. Chang, X. Lei, X. Sun, Chem. Commun. 49 (2013) 7516–7518.
[14] W. Yang, Y. Liu, Y. Hu, M. Zhou, H. Qian, J. Mater. Chem. 22 (2012) 13895–13898.
[15] A. Du, Z. Zhu, S.C. Smith, J. Am. Chem. Soc. 132 (2010) 2876–2877.
[16] J. Dai, X. Wu, J. Yang, X.C. Zeng, J. Phys. Chem. Lett. 5 (2014) 393–398.
[17] H. Zhang, C.-J. Tong, Y. Zhang, Y.-N. Zhang, L.-M. Liu, J. Mater. Chem. A 3 (2015) 9632–9637.
[18] P.V. Kamat, J. Phys. Chem. Lett. 2 (2011) 242–251.
[19] K. Maeda, K. Domen, J. Phys. Chem. Lett. 1 (2010) 2655–2661.
[20] I. Vurgaftman, J.R. Meyer, L.R. Ram-Mohan, J. Appl. Phys. 89 (2001) 5815–5875.
[21] R. Dingle, D.D. Sell, S.E. Stokowski, M. Ilegems, Phys. Rev. B 4 (1971) 1211–1218.
[22] C.L. Freeman, F. Claeyssens, N.L. Allan, J.H. Harding, Phys. Rev. Lett. 96 (2006) 066102.
[23] H. Zhang, Y.-N. Zhang, H. Liu, L.-M. Liu, J. Mater. Chem. A 2 (2014) 15389–15395.
[24] Z.Y. Al Balushi, K. Wang, R.K. Ghosh, R.A. Vila, S.M. Eichfeld, J.D. Caldwell, X. Qin, Y.-C. Lin, P.A. DeSario, G. Stone, S. Subramanian, D.F. Paul, R.M. Wallace, S. Datta, J.M. Redwing, J.A. Robinson, Nat. Mater. 15 (2016) 1166–1171.
[25] X. Li, Y.-W. Kim, P.W. Bohn, I. Adesida, Appl. Phys. Lett. 80 (2002) 980–982.
[26] F.K. Yam, Z. Hassan, L.S. Chuah, Y.P. Ali, Appl. Surf. Sci. 253 (2007) 7429–7434.
[27] F.K. Yam, Z. Hassan, A.Y. Hudeish, Thin Solid Films 515 (2007) 7337–7341.
[28] G. Kresse, J. Furthmüller, Phys. Rev. B 54 (1996) 11169–11186.
[29] G. Kresse, J. Furthmüller, Comput. Mater. Sci. 6 (1996) 15–50.
[30] J.P. Perdew, K. Burke, M. Ernzerhof, Phys. Rev. Lett. 77 (1996) 3865–3868.
[31] G. Kresse, D. Joubert, Phys. Rev. B 59 (1999) 1758–1775.
[32] H.J. Monkhorst, J.D. Pack, Phys. Rev. B 13 (1976) 5188–5192.
[33] A. Togo, F. Oba, I. Tanaka, Phys. Rev. B 78 (2008) 134106.
[34] K. Parlinski, Z.Q. Li, Y. Kawazoe, Phys. Rev. Lett. 78 (1997) 4063–4066.
[35] G. Brunetto, P.A.S. Autreto, L.D. Machado, B.I. Santos, R.P.B. dos Santos, D.S. Galvão, J. Phys. Chem. C. 116 (2012) 12810–12813.
[36] Y. Liu, G. Wang, Q. Huang, L. Guo, X. Chen, Phys. Rev. Lett. 108 (2012).
[37] D.C. Camacho-Mojica, F. López-Urías, Sci. Rep. 5 (2015) 17902.
[38] C. Persson, A. Ferreira da Silva, R. Ahuja, B. Johansson, J. Cryst. Growth 231 (2001) 397–406.
[39] Q. Li, D. Zhou, W.T. Zheng, Y.M. Ma, C.F. Chen, Phys. Rev. Lett. 110 (2013) 136403.
[40] W.-J. Yin, Y.-E. Xie, L.-M. Liu, R.-Z. Wang, X.-L. Wei, L. Lau, J.-X. Zhong, Y.-P. Chen, J. Mater. Chem. A 1 (2013) 5341–5346.
[41] H.L. Zhuang, R.G. Hennig, Chem. Mater. 25 (2013) 3232–3238.
[42] X. Huang, Z. Zeng, H. Zhang, Chem. Soc. Rev. 42 (2013) 1934–1946.
[43] A. Ramasubramaniam, Phys. Rev. B 86 (2012) 115409.
[44] J. Zhang, H. Zheng, R. Han, X. Du, Y. Yan, J. Alloy. Compd. 647 (2015) 75–81.
[45] D. Liu, Y. Guo, L. Fang, J. Robertson, Appl. Phys. Lett. 103 (2013) 183113.
[46] R.M. Sheetz, I. Ponomareva, E. Richter, A.N. Andriotis, M. Menon, Phys. Rev. B 80 (2009) 195314.
[47] G. Liu, L.-C. Yin, J.Q. Wang, P. Niu, C. Zhen, Y.P. Xie, H.-M. Cheng, Energy Environ. Sci. 5 (2012) 9603–9610.
[48] C.H. Sun, D.J. Searles, J. Phys. Chem. C. 117 (2013) 26454–26459.